Progress In Electromagnetics Research, PIER 103, 305–322, 2010

SCATTERING FROM LARGE 3-D PIECEWISE HOMOGENEOUS BODIES THROUGH LINEAR EMBEDDING VIA GREEN'S OPERATORS AND ARNOLDI BASIS FUNCTIONS

V. Lancellotti, B. P. de Hon, and A. G. Tijhuis

Department of Electrical Engineering
Technical University of Eindhoven
P. O. Box 513, Eindhoven 5600 MB, The Netherlands

Abstract—We apply the linear embedding via Green's operators (LEGO) method to the scattering by large finite dielectric bodies which contain metallic or penetrable inclusions. After modelling the body by means of LEGO bricks, we formulate the problem via an integral equation for the total incident currents over the boundaries of the bricks. This equation is turned into a weak form by means of the Method of Moments (MoM) and sub-domain basis functions. Then, to handle possibly large MoM matrices, we employ an order-reduction strategy based on: i) compression of the off-diagonal sub-blocks of the system matrix by the adaptive cross approximation algorithm and ii) subsequent compression of the whole matrix by using a basis of orthonormal entire-domain functions generated through the Arnoldi iteration algorithm. The latter leads to a comparatively small upper Hessenberg matrix easily inverted by direct solvers. We validate our approach and discuss the properties of the Arnoldi basis functions through selected numerical examples.

1. INTRODUCTION AND OVERVIEW

Nowadays, piecewise homogeneous media are ubiquitous in electrical engineering and physics, as they constitute a basic "ingredient" for countless electromagnetic (EM) and optical devices. For instance, frequency selective surfaces (FSS), electromagnetic and photonic band-gap structures, high impedance surfaces, printed antennas and the like are practical examples of structures which may involve a combination either of metallic and penetrable objects or of dielectric media with different properties, as sketched in Fig. 1.

Corresponding author: V. Lancellotti (v.lancellotti@tue.nl).

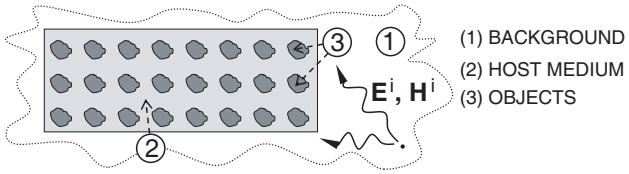

Figure 1. Scattering problem: A *finite* dielectric body (host medium) enclosing N_D (PEC or penetrable) identical objects is immersed in a homogeneous background medium and illuminated by incident fields.

Studying and designing such structures demands efficient and reliable numerical tools. Among these, domain decomposition methods (DDMs) based on boundary integral equations (BIEs) [1–5] turn out particularly efficient. In fact, when applied together with a suitable Method of Moments (MoM) [6] scheme, DDMs can effectively reduce the size of the resulting MoM matrix. This makes it affordable to solve the system with direct methods (e.g., `LU` factorization [7]), so as to circumvent slow convergence issues (sometimes encountered when using iterative methods for poor- or ill-conditioned systems).

Prior to applying any numerical scheme, DDMs try and reduce the complexity of the original EM problem by tearing the structure apart into small (interacting) domains. We are not aware, though, of DDMs which have been adapted to handle domains which include an object and whose filling (i.e., host) medium may exhibit EM properties different from the properties of the background, as shown in Fig. 2(a). Thereby, we propose an extension of the linear embedding via Green's operators (LEGO) method [8] for solving the scattering from large 3-D finite dielectric bodies which may include metallic or penetrable objects arranged in a regular pattern (Fig. 1). We mention that the recently proposed generalized surface integral equation (GSIE) formulation [5] can similarly handle large composite media (and possibly inhomogeneous at that). However, in [5] numerical examples are given for 2-D problems only.

The key point of LEGO is to model the structure in Fig. 1 as an aggregate of simply-shaped bricks $\mathcal{D}_k$, $k = 1, \ldots, N_D$, each one embedding (at least) one object [Fig. 2(a)]. The interior of $\mathcal{D}_k$ — which we think of as immersed in the background medium — is partly occupied by the object and partly filled with the host medium. This definition extends the notion of brick adopted in previous scattering [8–13] and antenna [14] problems, where, in contrast, background and host medium had the *same* properties. Finally, although we restrict our discussion to identical bricks, the approach we describe applies as well to a collection of possibly different bricks.

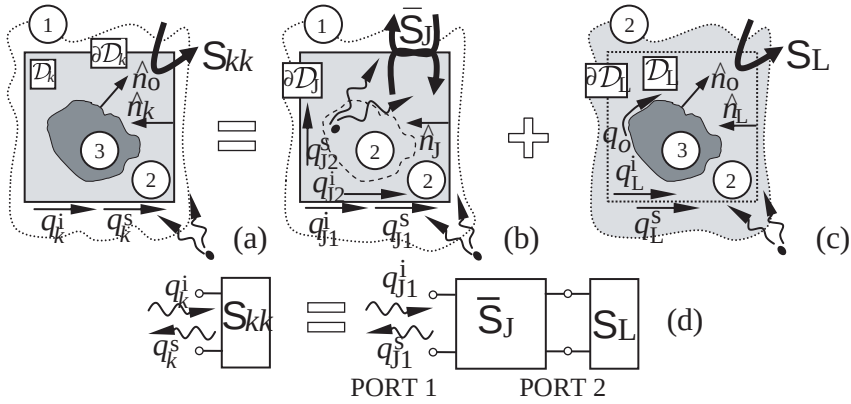

Figure 2. (a) A brick $\mathcal{D}_k = \partial\mathcal{D}_\mathrm{J} \cup \mathcal{D}_L$ carved out of the host medium and immersed in the background. (b) $\bar{\mathsf{S}}_\mathrm{J}$ accounts for the scattering by the material boundary $\partial\mathcal{D}_\mathrm{J}$. (c) S_L describes the scattering by $\mathcal{D}_L$. (d) Equivalent symbolic network representing the scattering from $\mathcal{D}_k$.

To formulate the problem in Fig. 1 with LEGO, we describe each brick $\mathcal{D}_k$ by a scattering operator S_{kk} (Section 2.1), and the interactions between any two bricks $\mathcal{D}_k$, $\mathcal{D}_n$ via transfer operators T_{kn} [8]. Then, unlike the approach we followed in [8, 11], we state an integral equation to be solved for the total incident current densities $q^{\mathrm{i}}_{k,\mathrm{tot}}$ (Section 2.2). That equation is reduced to a weak form (Section 3.1) via the standard MoM in Galerkin's form — Which may results in a relatively large matrix. Hence, to invert the system without resorting to iterative methods, we propose an order-reduction strategy hinging on

(i) Compression of the matrices $[T_{kn}] = [P^{\mathrm{i}}_{kk}]^{-1}[P_{kn}]$ [8], i.e., the algebraic counterparts of T_{kn}, via the adaptive cross approximation (ACA) algorithm [15, 16] applied to $[P_{kn}]$ (Section 3.2).

(ii) Compression of the whole system matrix by (formally) expanding $[q^{\mathrm{i}}_{\mathrm{tot}}]$ [8] on a basis of globally *entire-domain* basis functions generated through the Arnoldi iteration (Sections 3.3, 3.4).

The ACA algorithm, which exploits the rank-deficient nature of $[P_{kn}]$, enables us to reduce the memory occupancy of $[T_{kn}]$ as well as to fill it faster. In the second step above we apply the Arnoldi iteration [17] to a suitable sequence of vectors to obtain a set of N_A orthonormal vectors $[\psi_s]$, which we dub Arnoldi basis functions (ABFs) for short. Evidently, the entries of $[\psi_s]$ define a function whose support is $\cup_k \partial\mathcal{D}_k$. Then, we use $\{[\psi_s]\}$ to span the dominant subspace of $[q^{\mathrm{i}}_{\mathrm{tot}}]$ and turn the relevant equation (Section 3.4) into the final reduced-order

system. The relevant matrix is upper Hessenberg and it practically ensues from the Arnoldi iteration itself [17] — Which adds to the efficiency of the proposed strategy. Moreover, since in practice N_A is far lower than the number of Rao-Wilton-Glisson (RWG) functions [18] of the underlying MoM scheme, the reduced system can be inverted through `LU` factorization.

Lastly, in Section 4 we discuss the validation of the numerical code we developed, and we apply LEGO in its new form to the scattering from a finite FSS comprised of perfectly electrically conducting (PEC) thick square loops immersed in a host dielectric slab.

2. FORMULATION WITH LEGO

2.1. Scattering Operator of $\mathcal{D}_k$

We capture the EM behavior of $\mathcal{D}_k$ via its scattering operator S_{kk}, which links equivalent incident currents q_k^{i} to equivalent scattered currents q_k^{s} on $\partial\mathcal{D}_k$, viz.,

$$q_k^{\mathrm{s}} = \mathsf{S}_{kk} q_k^{\mathrm{i}}, \tag{1}$$

where $q_k^{\mathrm{s,i}}$ are defined in [8, Eq. (2)]. Notice that $q_k^{\mathrm{s,i}}$ are located at an infinitesimal distance from $\partial\mathcal{D}_k$ in the background medium [Fig. 2(a)]. One way of obtaining S_{kk} consists of posing a set of coupled BIEs on $\partial\mathcal{D}_k$ and the surface of the embedded object. However, we favor an alternative modular approach in line with the LEGO philosophy, i.e., we decompose $\mathcal{D}_k$ into the union of the material boundary $\partial\mathcal{D}_{\mathrm{J}} \equiv \partial\mathcal{D}_k$ plus the inner volume $\mathcal{D}_{\mathrm{L}} = \mathcal{D}_k \backslash \partial\mathcal{D}_{\mathrm{J}}$. Then, we tackle two auxiliary problems, namely:

(i) The EM scattering due to the material boundary $\partial\mathcal{D}_{\mathrm{J}}$ with the object inside $\mathcal{D}_k$ replaced by the host medium [Fig. 2(b)]. In this instance, on allowing for sources radiating from both sides of $\partial\mathcal{D}_{\mathrm{J}}$, we arrive at the scattering operator $\overline{\mathsf{S}}_{\mathrm{J}}$ of the discontinuity between background (labelled 1) and host medium (labelled 2).

(ii) The EM scattering off $\mathcal{D}_{\mathrm{L}}$ (which does include the object) when immersed in the host medium [Fig. 2(c)]. In this case, on placing sources outside $\partial\mathcal{D}_{\mathrm{L}}$ we simply derive S_{L} as in [8].

By definition $\overline{\mathsf{S}}_{\mathrm{J}}$ (a 2×2 abstract matrix of operators S_{Jlm}, $l, m \in \{1, 2\}$) maps scattered currents to incident currents on either side of $\partial\mathcal{D}_{\mathrm{J}}$, viz.

$$\begin{bmatrix} q_{\mathrm{J}1}^{\mathrm{s}} \\ q_{\mathrm{J}2}^{\mathrm{s}} \end{bmatrix} = \begin{bmatrix} \mathsf{S}_{\mathrm{J}11} & \mathsf{S}_{\mathrm{J}12} \\ \mathsf{S}_{\mathrm{J}21} & \mathsf{S}_{\mathrm{J}22} \end{bmatrix} \begin{bmatrix} q_{\mathrm{J}1}^{\mathrm{i}} \\ q_{\mathrm{J}2}^{\mathrm{i}} \end{bmatrix}, \tag{2}$$

where $q_{Jl}^{\mathrm{s,i}}$ are defined analogously to $q_k^{\mathrm{s,i}}$. For the sake of clarity, we defer the derivation of $\overline{\mathsf{S}}_{\mathrm{J}}$ to Appendix A.

It is possible to associate $\mathcal{D}_k$, $\mathcal{D}_{\mathrm{L}}$, $\partial\mathcal{D}_{\mathrm{J}}$ with (symbolic) lumped components whereby we represent the EM problem in Fig. 2(a) with the equivalent circuit in Fig. 2(d). In this network analogue the currents q play the role of power waves. Pushing the analogy farther, we can say that $\mathcal{D}_k$ is the cascade of $\partial\mathcal{D}_{\mathrm{J}}$ and $\mathcal{D}_{\mathrm{L}}$. Therefore, if we treat $\overline{\mathsf{S}}_{\mathrm{J}}$ and S_{L} like ordinary scattering matrices [19], we find

$$\mathsf{S}_{kk} = \overline{\mathsf{S}}_{\mathrm{J}} * \mathsf{S}_{\mathrm{L}} = \mathsf{S}_{\mathrm{J}11} + \mathsf{S}_{\mathrm{J}12}\mathsf{S}_{\mathrm{L}}(\mathsf{I}_{\mathrm{J}} - \mathsf{S}_{\mathrm{J}22}\mathsf{S}_{\mathrm{L}})^{-1}\mathsf{S}_{\mathrm{J}21}, \tag{3}$$

where $*$ denotes the Redheffer star product [20] and I_{J} is the identity operator on $\partial\mathcal{D}_{\mathrm{J}}$ (see Table A1). In the notable case when no object exists within $\mathcal{D}_k$, then $\mathsf{S}_{\mathrm{L}} = 0$ and (3) simplifies to $\mathsf{S}_{kk} \equiv \mathsf{S}_{\mathrm{J}11}$.

We observe that, if we were to solve a scattering problem as the one shown in Fig. 1 with the same host medium but different inclusions (as long as this does not entail changing the shape of $\partial\mathcal{D}_k$), then we would only have to re-compute S_{L} and carry out the cascade (3). Dual considerations hold if we allow the EM properties of the background to vary, while keeping the host medium and the inclusions unchanged.

2.2. Derivation of the Integral Equations

When we take into account the multiple scattering amongst the N_D bricks modeling the structure in Fig. 1, (1) generalizes to [8]

$$q_k^{\mathrm{s}} = \mathsf{S}_{kk} q_{k,\mathrm{tot}}^{\mathrm{i}}, \qquad q_{k,\mathrm{tot}}^{\mathrm{i}} = q_k^{\mathrm{i}} + \sum_{n\neq k}^{N_D} \mathsf{T}_{kn} q_n^{\mathrm{s}}, \tag{4}$$

where we have introduced the total incident currents $q_{k,\mathrm{tot}}^{\mathrm{i}}$ and the transfer operators T_{kn} [8, Eq. (15)]. To state an equation for $q_{k,\mathrm{tot}}^{\mathrm{i}}$, we plug the first of (4) into the second of (4) and we eliminate q_k^{s}. Then, by organizing q_k^{i} ($q_{k,\mathrm{tot}}^{\mathrm{i}}$) into a column vector q^{i} ($q_{\mathrm{tot}}^{\mathrm{i}}$), we arrive at

$$q_{\mathrm{tot}}^{\mathrm{i}} = q^{\mathrm{i}} + \mathsf{T}\,\mathrm{diag}\{\mathsf{S}_{nn}\} q_{\mathrm{tot}}^{\mathrm{i}}, \tag{5}$$

where the total transverse operator T is a square matrix with entries

$$(\mathsf{T})_{kn} = \begin{cases} 0, & n = k, \\ \mathsf{T}_{kn} = (\mathsf{P}_{kk}^{\mathrm{i}})^{-1}\mathsf{P}_{kn}, & n \neq k, \end{cases} \quad k, n = 1, \ldots, N_D, \tag{6}$$

and the propagators $\mathsf{P}_{kk}^{\mathrm{i}}$, P_{kn} are listed in [8, Table 1]. Eventually, once $q_{k,\mathrm{tot}}^{\mathrm{i}}$ are known, we can determine q_k^{s} from the leftmost of (4).

3. NUMERICAL SOLUTION

3.1. Reduction to Weak Form Via MoM

To solve (5) we first calculate the algebraic counterparts of S_{nn} and T_{kn} [8] through the MoM in Galerkin's form [6]. To this purpose, we

model $\partial\mathcal{D}_k$ with a regular 3-D triangular patching on which we define two sets of RWG basis functions [18] $\{\mathbf{f}_{kp}\}$, $\{\mathbf{g}_{kp}\}$, $p = 1, \ldots, N_F$, to represent $q_k^{\mathrm{s,i}}$. The current q_{o} induced on the object inside $\mathcal{D}_k$ [Fig. 2(c)] is represented by a suitable set of N_O RWG functions: Definitions and details can be found in [8]. Finally, the total incident currents are expanded as

$$q^{\mathrm{i}}_{k,\mathrm{tot}} = \begin{bmatrix} \sqrt{\eta_1}\mathbf{J}^{\mathrm{i}}_{k,\mathrm{tot}} \\ -\mathbf{M}^{\mathrm{i}}_{k,\mathrm{tot}}/\sqrt{\eta_1} \end{bmatrix} = \sum_{p=1}^{N_F} \begin{bmatrix} \mathbf{f}_{kp} J^{\mathrm{i}}_{kp,\mathrm{tot}} \\ -\mathbf{g}_{kp} M^{\mathrm{i}}_{kp,\mathrm{tot}} \end{bmatrix}, \tag{7}$$

where $\eta_1 = \sqrt{\varepsilon_1/\mu_1}$ is the intrinsic impedance of the background medium, and we have included $\sqrt{\eta_1}$ within $J^{\mathrm{i}}_{kp,\mathrm{tot}}$, $M^{\mathrm{i}}_{kp,\mathrm{tot}}$. With these preliminaries, the weak form of (5) and the first of (4) reads

$$[q^{\mathrm{i}}_{\mathrm{tot}}] = [q^{\mathrm{i}}] + [T]\,\mathrm{diag}\{[S_{nn}]\}[q^{\mathrm{i}}_{\mathrm{tot}}], \quad [q^{\mathrm{s}}] = \mathrm{diag}\{[S_{kk}]\}[q^{\mathrm{i}}_{\mathrm{tot}}], \tag{8}$$

with

$$([T])_{kn} = \begin{cases} [0]\,, & n = k, \\ [T_{kn}] = [P^{\mathrm{i}}_{kk}]^{-1}[P_{kn}]\,, & n \neq k, \end{cases} \quad k, n = 1, \ldots, N_D, \tag{9}$$

where with transparent notation each matrix denotes the algebraic counterpart of the corresponding operator. The rank of $[T]\,\mathrm{diag}\{[S_{nn}]\}$ is $2N_F N_D$.

3.2. Compression of $[P_{kn}]$ via Adaptive Cross Approximation

The propagator $[P_{kn}]$ in (9) possesses the block structure [8]

$$[P_{kn}] = \begin{bmatrix} [0] & [0] \\ [P_{kn}]_{\mathrm{HJ}} & [P_{kn}]_{\mathrm{HM}} \end{bmatrix}, \quad n \neq k, \tag{10}$$

where each sub-matrix has size $N_F \times N_F$. The subscripts HJ (HM) signify that (within an immaterial normalization constant) the entries of $[P_{kn}]_{\mathrm{HJ}}$ ($[P_{kn}]_{\mathrm{HM}}$) constitute the reaction [21, 22] between the tangential magnetic field — generated by the elemental current $\mathbf{f}_{np}$ ($\mathbf{g}_{np}$) on $\partial\mathcal{D}_n^-$ — and the elemental current $\mathbf{f}_{kq}$ ($\mathbf{g}_{kq}$), $q = 1, \ldots, N_F$, on $\partial\mathcal{D}_k^+$. Thereby, based on the classical multipole expansion [23], the entries of $[P_{kn}]_{\mathrm{H}\alpha}$, $\alpha = \mathrm{J}, \mathrm{M}$, can be proven to decay to zero, when the distance between $\mathcal{D}_k$ and $\mathcal{D}_n$ is increased. Besides, under the same circumstances, the magnetic field should exhibit only small variations over $\partial\mathcal{D}_k$. The latter two effects combined together cause the columns of $[P_{kn}]_{\mathrm{H}\alpha}$ to become almost linearly dependent.

At any rate, in line with this, a singular value decomposition [7] reveals that the higher-order singular values of $[P_{kn}]_{\mathrm{H}\alpha}$ are practically null. This means that we can store the "information" contained in

$[P_{kn}]_{\mathrm{H}\alpha}$ with far fewer entries than the actual $2N_F^2$ in (10), while preserving the accuracy of $[T_{kn}]$. To this end, we apply the ACA algorithm [15, 16] which allows us to factorize $[P_{kn}]_{\mathrm{H}\alpha}$ as

$$[P_{kn}]_{\mathrm{H}\alpha} \approx [U_{kn}]_{\mathrm{H}\alpha}\, [V_{kn}]_{\mathrm{H}\alpha}\,, \tag{11}$$

where $[U_{kn}]_{\mathrm{H}\alpha}$ ($[V_{kn}]_{\mathrm{H}\alpha}$) is of size $N_F \times N_{\alpha(kn)}$ ($N_{\alpha(kn)} \times N_F$).

Now, the number of matrices $[P_{kn}]$ to be computed is at most $N_{T,\max} = N_D(N_D-1)/2$, because $[P_{nk}]_{\mathrm{H}\alpha} = [P_{kn}]^T_{\mathrm{H}\alpha}$ due to reciprocity [22]. Hence, storing the ACA decomposed matrices $[P_{kn}]$ (the null entries need not be stored) requires a grand total

$$N_L = 2N_F \sum_{k=1}^{N_D} \sum_{n=k+1}^{N_D} \left(N_{\mathrm{J}(kn)} + N_{\mathrm{M}(kn)}\right), \tag{12}$$

complex double-precision floating-point memory locations. This number has to be contrasted with $4N_F^2 \times 2N_T$, i.e., the memory locations needed for the full storage of $[T]$ (which is *not* symmetric).

Notice that in (12) we assume all of the $[P_{kn}]$ to differ from one another, viz., the worst case scenario — which occurs for an arbitrary distribution of bricks in the background medium. Actually, if the bricks are to model a dielectric body with a regular distribution of inclusions (as in Fig. 1), then $[P_{kn}]$ (and hence $[T_{kn}]$) come in clusters of equal matrices, and hence $N_T \ll N_{T,\max}$. Obviously, we do not compute the same transfer matrix more than once, nor do we store it over and over again: This results in both time and memory saving.

3.3. Generation of the Arnoldi Basis Functions

As suggested by the first of (8), a set of vectors well suited for expanding $[q^{\mathrm{i}}_{\mathrm{tot}}]$ may be the sequence

$$\left\{ \left([T]\,\mathrm{diag}\{[S_{nn}]\}\right)^{s-1}[q^{\mathrm{i}}] \right\}_{s=1}^{N_A}, \tag{13}$$

which defines a Krylov subspace $\mathcal{K}_{N_A}$ [24] of order N_A for the matrix $[T]\,\mathrm{diag}\{[S_{nn}]\}$. The vectors (13), though, are known to grow ever more linearly dependent as N_A is increased — Which renders them less attractive as a basis. To get around this problem, from (13) we generate an orthonormal basis $\{[\psi_s]\}_{s=1}^{N_A}$ through the Arnoldi iteration [17], which is essentially a stabilized Gram-Schmidt algorithm [7]. For the sake of completeness, in Table 1, we list the steps of the Arnoldi iteration tailored to (13). The iteration also yields an upper Hessenberg matrix $[H_{N_A}]$ of rank N_A, which in our notation reads

$$[H_{N_A}] = [\Psi_{N_A}]^H\, [T]\,\mathrm{diag}\{[S_{nn}]\}\,[\Psi_{N_A}]\,, \tag{14}$$

Table 1. Pseudo-code of the Arnoldi iteration algorithm.

	Notes
1. $[\psi_1] := [q^{\mathrm{i}}]/\|[q^{\mathrm{i}}]\|_2$	$\|\cdot\|$ denotes the 2-norm in the space spanned by the columns of $[T]\,\mathrm{diag}\{[S_{nn}]\}$.
2. for $v = 2, \ldots, N_A + 1$	$h_{u,v}$ stands for the entry uv of $[H_{N_A}]$.
i. $[\psi_v] := [T]\,\mathrm{diag}\{[S_{nn}]\}\,[\psi_{v-1}]$	For $v = N_A + 1$ step 2.iii yields $h_{N_A+1,\,N_A}$ which is discarded, as it does not belong to $[H_{N_A}]$.
ii. for $u = 1, \ldots, v-1$	
• $h_{u,\,v-1} := [\psi_u]^H\,[\psi_v]$	
• $[\psi_v] := [\psi_v] - h_{u,\,v-1}\,[\psi_u]$	
iii. $h_{v,\,v-1} := \|[\psi_v]\|_2$	
iv. $[\psi_v] := [\psi_v]/h_{v,\,v-1}$	

where $[\Psi_{N_A}]$ (of size $2N_F N_D \times N_A$) stores $[\psi_s]$ columnwise.

It is worthwhile elaborating a bit on the calculation of

$$[\psi_s] = [T]\,\mathrm{diag}\{[S_{nn}]\}\,[\psi_{s-1}]\,, \quad s = 1, \ldots, N_A \tag{15}$$

i.e., the matrix-by-vector multiplications which are instrumental to the Arnoldi iteration (step 2.i of the algorithm in Table 1). Specifically, upon letting $([\psi_s])_k = [\psi_{ks}]$ and using (10), (11), we cast (15) into

$$\left[P^{\mathrm{i}}_{kk}\right][\psi_{ks}] \approx \sum_{n\neq k}^{N_D} \begin{bmatrix} [0] & [0] \\ [U_{kn}]_{\mathrm{HJ}}\,[V_{kn}]_{\mathrm{HJ}} & [U_{kn}]_{\mathrm{HM}}\,[V_{kn}]_{\mathrm{HM}} \end{bmatrix} [S_{nn}]\,[\psi_{n\,s-1}]\,, \tag{16}$$

for $k, n = 1, \ldots, N_D$. Now, proceeding from right to left, we first compute $[S_{nn}]\,[\psi_{n\,s-1}]$. The resulting vector is then left-multiplied by $[V_{kn}]_{\mathrm{H}\alpha}$, and the result is in turn left-multiplied by $[U_{kn}]_{\mathrm{H}\alpha}$. Thus, at each step we just need a buffer array of length (no more than) $2N_F$ to store and add up the partial results. At last, when we are done with the right hand side of (16), we get $[\psi_{ks}]$ by inverting $[P^{\mathrm{i}}_{kk}]$ through a $\mathtt{U}\mathtt{U}^T$ decomposition [25]. All of these operations are to be repeated $\forall k$.

3.4. Order Reduction

To proceed, we expand $[q^{\mathrm{i}}_{\mathrm{tot}}]$ in the basis $\{[\psi_s]\}_{s=1}^{N_A}$, viz.,

$$[q^{\mathrm{i}}_{\mathrm{tot}}] = [\Psi_{N_A}]\,[a]\,, \quad [a] = [a_1, \ldots, a_{N_A}]^T\,. \tag{17}$$

By substituting (17) into the first of (8), left-multiplying both sides by $[\Psi_{N_A}]^H$, and taking advantage of (14), we obtain

$$([I] - [H_{N_A}])\,[a] = [\Psi_{N_A}]^H\,[q^{\mathrm{i}}], \tag{18}$$

where the system matrix is of size $N_A \times N_A$ and still upper Hessenberg. Since $[H_{N_A}]$ comes for free, as a by-product of the Arnoldi iteration, no more heavy calculations are in order to fill the system matrix in (18). Lastly, in the light of (17) and (18) the total incident currents can be formally written as

$$[q^{\mathrm{i}}_{\mathrm{tot}}] = [\Psi_{N_A}] \left([I] - [H_{N_A}]\right)^{-1} [\Psi_{N_A}]^H [q^{\mathrm{i}}], \tag{19}$$

while the scattered currents ensue from the second of (8). In practice, the required number of ABFs satisfies $N_A \ll 2N_F N_D$, and hence (19) constitutes a notable compression of the MoM system (8).

We conclude emphasizing that the Arnoldi iteration merely serves the purpose of generating the vectors $[\psi_s]$, hence the proposed strategy is no iterative method.

4. NUMERICAL RESULTS

We have implemented the numerical solution of (18) in a code able to handle arbitrarily shaped bricks enclosing PEC or penetrable inclusions. The validation campaign entails assessing 1) the calculation of $\overline{\mathsf{S}}_{\mathrm{J}}$ and 2) the correctness and accuracy of the order reduction based on the ACA algorithm and the ABFs.

As regards the first issue above, we have studied the scattering by a solitary dielectric cubic brick ($2N_F = 1152$) which embeds a PEC sphere ($N_O = 588$), as shown in Fig. 3. For this problem we have derived a reference solution ($q^{\mathrm{s}}_{1,\mathrm{MoM}}$) by solving a set of coupled PMCHW equations (over $\partial\mathcal{D}_1$) and EFIE (over the sphere) via the MoM. The LEGO solution relies on (1), with S_{11} computed via (3), and on (A4), based on PMCHW equations. In Fig. 3, we have plotted the radar cross section (RCS) obtained with LEGO ($\bullet$) and the reference data ($-/--$). The curves are practically indistinguishable, which confirms the validity of (3) and (A4). To shed light on the pointwise accuracy of q^{s}_1, for the same frequency ($d = 0.5\lambda_2$) in Fig. 5, we have plotted the local deviation with respect to the reference solution, viz.,

$$\epsilon^{(1)}_r \stackrel{\mathrm{def}}{=} |([q^{\mathrm{s}}_1])_r - ([q^{\mathrm{s}}_{1,\mathrm{MoM}}])_r| / \parallel [q^{\mathrm{s}}_{1,\mathrm{MoM}}] \parallel_2, \quad r = 1, \ldots, 2N_F, \tag{20}$$

with $\| \cdot \|_2$ denoting the vector 2-norm [25] in the space spanned by the columns of $[S_{11}]$. Since $\epsilon^{(1)}_r$ does not exceed $\approx 18 \cdot 10^{-4}$ (0.18%) over $\partial\mathcal{D}_1$, the scattered currents are indeed correctly represented.

Secondly, to validate (19) we have investigated the scattering by a dielectric slab (edge $2d$, height h) which includes four infinitely-thin PEC crosses (length a, width t) arranged in a regular rectangular pattern, as shown in Fig. 4. We model the slab with $N_D = 4$

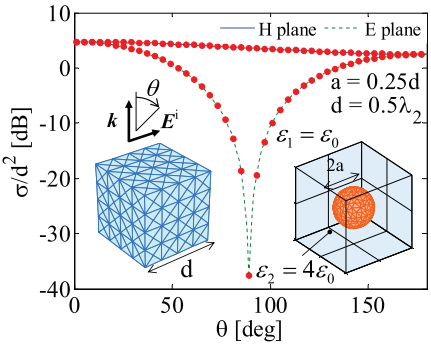

Figure 3. LEGO validation: RCS of a cubic dielectric shell embedding a PEC sphere; LEGO solution (•) versus MoM solution (−−/−). Insets: triangular-facet models of the cubic shell and the sphere, and incident plane wave.

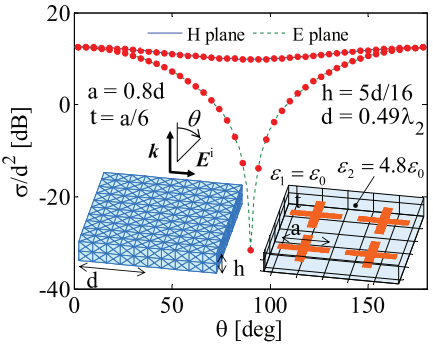

Figure 4. LEGO validation: RCS of a dielectric slab embedding four PEC crosses; LEGO solution (•) with $N_D = 4$, $N_A = 30$ versus MoM solution (−−/−). Insets: triangular-facet models of the bricks and the crosses, and incident plane wave.

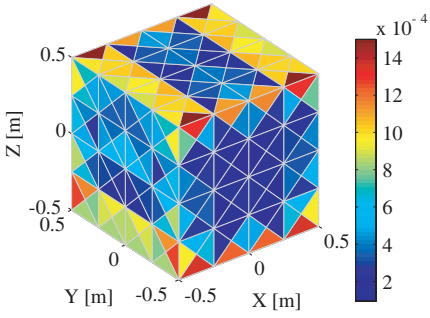

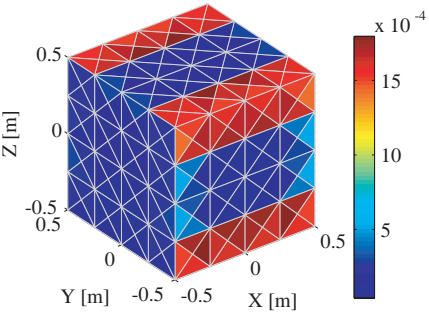

Figure 5. LEGO validation: local deviation $\epsilon_r^{(1)}$ of q_1^s computed through LEGO with respect to MoM solution for the cubic shell in Fig. 3; the electric (magnetic) part of $\epsilon_r^{(1)}$ is shown on left (right).

bricks each containing one cross. For this problem, $N_O = 277$, $2N_F = 1080$, $N_A = 50$, and the ranks of $[T]\,\mathrm{diag}\{S_{nn}\}$ and $[H_{N_A}]$ are 4320 and 50, respectively. Again, we obtain a reference solution by applying the MoM to a set of coupled PMCHW equations (over the slab's surface, 3360 RWG functions) and EFIE (over the crosses, 1108 RWG functions). The RCS calculated through the two methods are superimposed in Fig. 4 as well: the results are in excellent agreement,

Table 2. Ranks of $[U_{kn}]_{\mathrm{H}\alpha}$, $[V_{kn}]_{\mathrm{H}\alpha}$ relevant to the slab in Fig. 4.

n	k	τ_{kn}/d	$[U_{kn}]_{\mathrm{HJ}}$, $[V_{kn}]_{\mathrm{HJ}}$	$[U_{kn}]_{\mathrm{HM}}$, $[V_{kn}]_{\mathrm{HM}}$
1	2	1	187	163
1	3	1	197	173
1	4	1.414	128	129
2	3	1.414	127	126

thus validating both the implementation of the ACA algorithm and the generation of the ABFs.

Concerning this, the threshold t_A for stopping the ACA [16] of $[P_{nk}]$ was conservatively set to 10^{-5}; the corresponding ranks of the rectangular matrices $[U_{kn}]_{\mathrm{H}\alpha}$ and $[V_{kn}]_{\mathrm{H}\alpha}$ are listed in Table 2 as a function of the relative distance τ_{kn}/d among the bricks. These numbers are remarkably lower than the actual rank of $[P_{kn}]_{\mathrm{H}\alpha}$, i.e., $N_F = 540$. Moreover, the larger the separation of two bricks, the smaller the rank of $[U_{kn}]_{\mathrm{H}\alpha}$ and $[V_{kn}]_{\mathrm{H}\alpha}$ — As observed in [16] for the off-diagonal sub-blocks of the MoM matrix arising from an EFIE. Thus, to make the most out of the ACA in terms of memory occupation, it may be advisable to choose t_A adaptively, that is, larger (smaller) values for farther (nearer) bricks. Finally, in view of the finite translational symmetry of the slab, we need to compute and store only $N_T = 4 < N_{T,\max} = 6$ propagators, as anticipated in Section 3.2.

As for the convergence of q^{s}, in Fig. 6 we have plotted the expansion coefficients a_s versus their index. It is seen that the a_s drop to the threshold of numerical noise for $s = 44$ and that the decay rate is exponential. To assess the global accuracy of the solution, we have solved (18) with an increasing number of ABFs, namely, $N_A \in \{5, 10, 15, 20, 25, 30\}$. Then, for each test we have determined the 2-norm relative error on $[q^{\mathrm{i}}_{\mathrm{tot}}]$, viz.,

$$\delta_{q^{\mathrm{i}}_{\mathrm{tot}}} \stackrel{\mathrm{def}}{=} \| \, [\, \| \, q^{\mathrm{i}}_{\mathrm{tot}}] - [q_{\mathrm{ref}}]_2 \, / \, \| \, [q_{\mathrm{ref}}] \, \|_2, \tag{21}$$

where now $\| \cdot \|_2$ denotes the vector 2-norm in the space spanned by the rows of $[T]\,\mathrm{diag}\{[S_{nn}]\}$, and $[q_{\mathrm{ref}}] \equiv [q^{\mathrm{i}}_{\mathrm{tot}}]$ obtained with $N_A = 50$ — which we reckon "exact" in view of Fig. 6. Fig. 4 shows $\delta_{q^{\mathrm{i}}_{\mathrm{tot}}}$ versus the number of employed ABFs: apparently, 15 ABFs are sufficient to compute $q^{\mathrm{i}}_{\mathrm{tot}}$ with an error of about 0.01%.

In the various numerical experiments conducted so far, we have noticed that the a_s are mostly affected by the contrast between the background and the host medium and by the frequency. In general, the a_s oscillate until they start decaying nearly exponentially: Sharper contrasts and higher frequencies delay the onset of the exponential

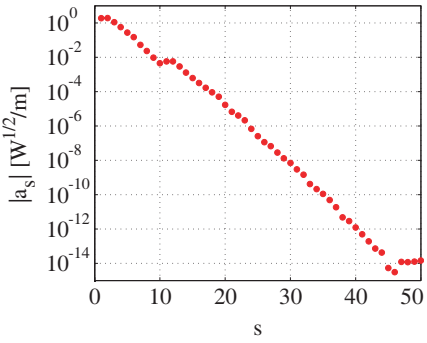

Figure 6. Expansion coefficients of $q^{\mathrm{i}}_{\mathrm{tot}}$ in the basis of ABFs vs. their index for the slab in Fig. 4.

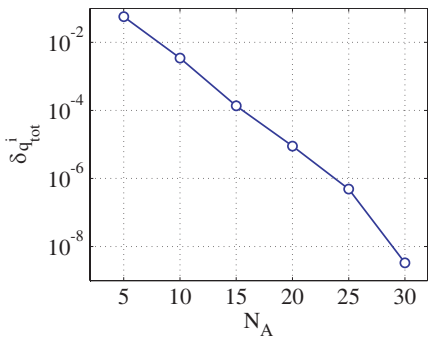

Figure 7. 2-norm error on $[q^{\mathrm{i}}_{\mathrm{tot}}]$ vs. the number of ABFs used to solve (18) for the slab in Fig. 4.

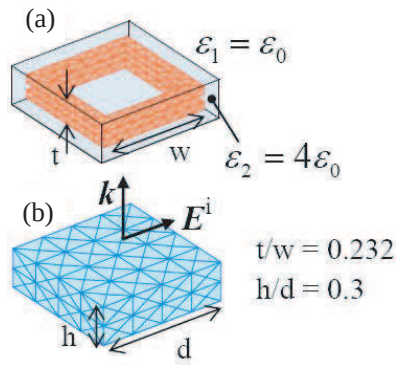

Figure 8. Triangular-facet model of the unit cell of a 10-by-10 two-layer FSS: (a) two thick PEC square loops and (b) LEGO brick.

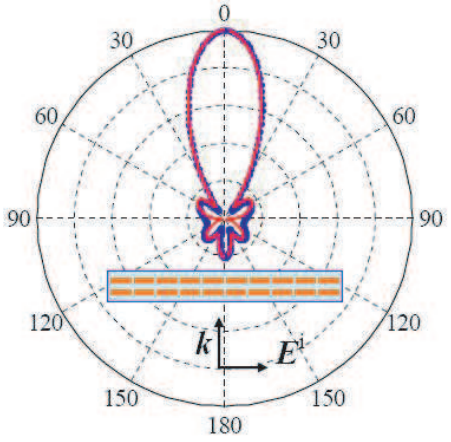

Figure 9. Normalized radiation pattern of the FSS at resonance ($4w/\lambda_2 = 1.008$): ($-$) E-plane, ($\bullet$) H-plane. Inset: side view of the FSS and incident plane wave.

convergence and reduce the decay rate as well. In addition, N_A also seems to be affected by N_D (ultimately, the rank of $[T]\,\mathrm{diag}\{S_{nn}\}$).

We conclude describing the application of LEGO to an FSS (e.g., see [26]) comprised of 200 PEC thick square loops (average edge $w = 7.75\,\mathrm{mm}$) embedded in a dielectric host medium ($\varepsilon_2 = 4\varepsilon_0$) and arranged on two parallel planes (distance $t = 0.232w$) in a 10×10

regular square lattice. As a LEGO brick we assume the unit cell (edge $d = 10\,\text{mm}$, height $h = 0.3d$), which contains two loops, as shown in Fig. 8. For these experiments, $N_D = 100$, $N_O = 672$ and $2N_F = 768$. Hence, the rank of $[T]\,\text{diag}\{S_{nn}\}$ is 76800, whereas a direct MoM solution would require inverting a matrix size $(N_O + 2N_F)N_D = 144000$. In contrast, we employed just $N_A = 600$ ABFs.

We solved (19) for 21 frequency samples evenly distributed from 4.5 to 5.25 GHz. Shown in Fig. 9 is the normalized radiation pattern of the FSS in response to a plane wave impinging normally at the frequency $f = 4.875\,\text{GHz}$. At such frequency the loops resonate, and the FSS lets most of the power go through. This is confirmed by the plot of the transmitted and back-scattered RCS versus the loops' electric length (Fig. 10): It is seen that there is a minimum (maximum) of reflection (transmission) for $4w = 1.008\lambda_2$, with λ_2 the wavelength in the host medium.

The calculations were carried out on a Linux-based x86_64 workstation equipped with an Intel Xeon 2.66-GHz processor and 8-GB RAM. We set the threshold t_A for the ACA algorithm to 10^{-4}. Then, for a single frequency sample, the average time spent computing $N_T = 180$ propagator matrices $[P_{kn}]$ (out of $N_{T,\max} = 4950$, in view of the limited translational symmetry of the FSS) was $\approx 54\,\text{s}$, while the time needed to build the ABFs was about 57 mins. The latter is mostly affected by the ranks of $[T]\,\text{diag}\{[S_{nn}]\}$ and of the ACA-reduced matrices used to approximate $[P_{kn}]$, as given by (11).

It should be noted that $N_A = 600$ ABFs are quite an overkill for the lower frequency values we considered, whereas they are necessary

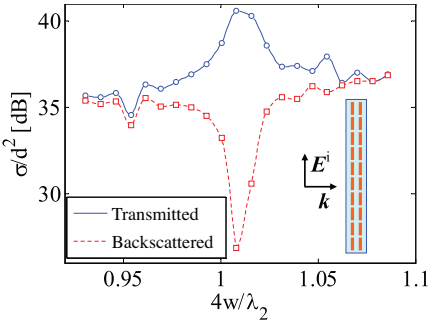

Figure 10. RCS of the FSS. Inset: side view of the FSS and incident plane wave.

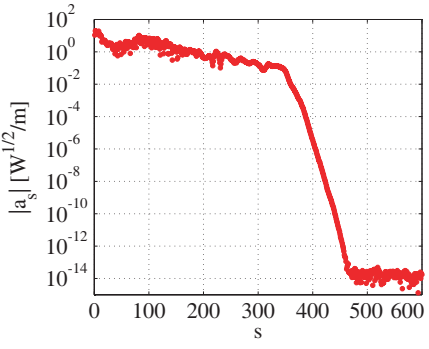

Figure 11. Expansion coefficients of $q^{\text{i}}_{\text{tot}}$ in the basis of ABFs vs. their index for the FSS at resonance ($4w/\lambda_2 = 1.008$).

to attain a reasonable level of convergence of a_s for the higher values. For instance, as is evident from Fig. 11, at the resonance just 400 ABFs would suffice to achieve values of $|a_s|$ as small as $\approx 10^{-7}|a_1|$. Therefore, adaptively choosing N_A would allow the computational time to be reduced.

5. CONCLUSION AND OUTLOOK

We have discussed an order-reduction strategy which — combined with LEGO — allows us to solve relatively large 3-D scattering problems involving piecewise homogeneous finite bodies. The key steps are the compression of the rank-deficient off-diagonal blocks of the relevant system matrix *and* the overall reduction in size by means of ad-hoc generated entire-domain functions (ABFs). This strategy has the potential of reducing the computational burden also in the study of the scattering by large dielectric bodies with no inclusions, though possibly pointwise inhomogeneous (e.g., as in [5]), by simply "dicing" the structure into small bricks. A detailed study of the dependence of the ABFs on the frequency, the shape and the content of the bricks, as well as on the number of bricks modelling a body, is still ongoing and the results will be the subject of a forthcoming paper.

APPENDIX A. CALCULATION OF $\bar{\mathsf{S}}_{\mathrm{J}}$

Upon applying Love's equivalence principle [27] four times, as outlined in Fig. A1, on either side of $\partial\mathcal{D}_{\mathrm{J}}$ we introduce the following equivalent scattered and incident currents

$$q_{\mathrm{J}l}^{\mathrm{s,i}} = \begin{bmatrix} \mathbf{J}_l^{\mathrm{s,i}}\sqrt{\eta_l} \\ -\mathbf{M}_l^{\mathrm{s,i}}/\sqrt{\eta_l} \end{bmatrix}, \quad l = \begin{cases} 1: & \text{background medium} \\ 2: & \text{host medium} \end{cases} \tag{A1}$$

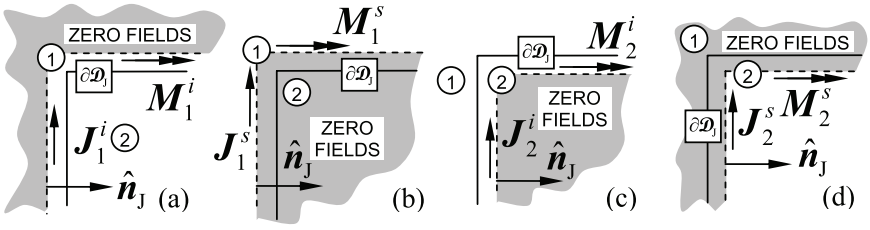

Figure A1. Four-fold application of Love's EP over the material boundary $\partial\mathcal{D}_{\mathrm{J}}$ for defining the equivalent incident and scattered currents (a), (b) in medium 1 and (c), (d) in medium 2.

Table A1. Operators used for defining $\overline{\mathsf{S}}_{\mathrm{J}}$ in (A4).

$G_l(R)$, $l=1,2$, is the 3-D scalar Green's function [22] in medium l. The unit normal $\hat{n}_{\mathrm{J}}$ to $\partial\mathcal{D}_k \equiv \partial\mathcal{D}_{\mathrm{J}} \equiv \partial\mathcal{D}_{\mathrm{L}}$ points *inward* $\mathcal{D}_k$ (Fig. A1).

NOMENCLATURE

$G_l(R)=\exp(-\mathrm{j}k_lR)/(4\pi R)$, $R=|\mathbf{r}-\mathbf{r}'|$, $k_l=\omega\sqrt{\varepsilon_l\mu_l}$,
$z_l=1/y_l=\eta_l/\eta_0$, $\underline{\underline{I}}_{\mathrm{s}}=\underline{\underline{I}}-\hat{n}_{\mathrm{J}}\hat{n}_{\mathrm{J}}$, $\nabla_{\mathrm{s}}=\underline{\underline{I}}_{\mathrm{s}}\cdot\nabla=\nabla-\hat{n}_{\mathrm{J}}(\hat{n}_{\mathrm{J}}\cdot\nabla)$,
$\nabla'_{\mathrm{s}}=-\nabla_{\mathrm{s}}$

BASIC RANK-2 DYADIC OPERATORS

$$\mathcal{L}_l=-\mathrm{j}\int_{\partial\mathcal{D}_{\mathrm{J}}}\mathrm{d}^2r'\left[k_lG_l(R)\underline{\underline{I}}_{\mathrm{s}}+\tfrac{1}{k_l}\nabla_{\mathrm{s}}G_l(R)\nabla'_{\mathrm{s}}\right]\cdot,\quad \mathbf{r}\in\partial\mathcal{D}_{\mathrm{J}}$$

$$\mathcal{K}_l^{\pm}=\text{P.V.}\int_{\partial\mathcal{D}_{\mathrm{J}}}\mathrm{d}^2r'\nabla'_{\mathrm{s}}G_l(R)\times\underline{\underline{I}}_{\mathrm{s}}\cdot\pm\tfrac{1}{2}\hat{n}_{\mathrm{J}}\times\underline{\underline{I}}_{\mathrm{s}}\cdot,\quad \mathbf{r}\in\partial\mathcal{D}_{\mathrm{J}}$$

PMCHW equations

$$\mathsf{W}=\begin{bmatrix} z_1\mathcal{L}_1+z_2\mathcal{L}_2 & -(\mathcal{K}_1^-+\mathcal{K}_2^+)\\ -(\mathcal{K}_1^-+\mathcal{K}_2^+) & -(y_1\mathcal{L}_1+y_2\mathcal{L}_2)\end{bmatrix},\quad \mathsf{C}_l=\begin{bmatrix}\underline{\underline{I}}_{\mathrm{s}}\cdot & 0\\ 0 & \underline{\underline{I}}_{\mathrm{s}}\cdot\end{bmatrix},\quad \sigma=1$$

Müller equations

$$\mathsf{W}=\begin{bmatrix}\varepsilon_1z_1\mathcal{L}_1-\varepsilon_2z_2\mathcal{L}_2 & -(\varepsilon_1\mathcal{K}_1^+-\varepsilon_2\mathcal{K}_2^-)\\ -(\mu_1\mathcal{K}_1^+-\mu_2\mathcal{K}_2^-) & -(\mu_1y_1\mathcal{L}_1-\mu_2y_2\mathcal{L}_2)\end{bmatrix},\ \mathsf{C}_l=\begin{bmatrix}\varepsilon_l\underline{\underline{I}}_{\mathrm{s}}\cdot & 0\\ 0 & \mu_l\underline{\underline{I}}_{\mathrm{s}}\cdot\end{bmatrix},\quad \sigma=-1$$

$$\Pi_{11}^{\mathrm{i}}=\begin{bmatrix}\sqrt{z_1}\mathcal{L}_1 & -\sqrt{z_1}\mathcal{K}_1^+\\ -\sqrt{y_1}\mathcal{K}_1^+ & -\sqrt{y_1}\mathcal{L}_1\end{bmatrix},\quad \Pi_{22}^{\mathrm{i}}=\begin{bmatrix}\sqrt{z_2}\mathcal{L}_2 & -\sqrt{z_2}\mathcal{K}_2^-\\ -\sqrt{y_2}\mathcal{K}_2^- & -\sqrt{y_2}\mathcal{L}_2\end{bmatrix}$$

$$\mathsf{D}_l=\begin{bmatrix}\sqrt{z_l}\underline{\underline{I}}_{\mathrm{s}}\cdot & 0\\ 0 & \sqrt{y_l}\underline{\underline{I}}_{\mathrm{s}}\cdot\end{bmatrix},\quad \mathsf{I}_{\mathrm{J}}=\begin{bmatrix}\underline{\underline{I}}_{\mathrm{s}}\cdot & 0\\ 0 & \underline{\underline{I}}_{\mathrm{s}}\cdot\end{bmatrix}$$

where $\eta_l=\sqrt{\mu_l/\varepsilon_l}$ is the intrinsic impedance in the corresponding medium. Then, over $\partial\mathcal{D}_{\mathrm{J}}$ we state a set of PMCHW [28] or Müller [29] BIEs which we solve for $\mathbf{J}=-\hat{n}_{\mathrm{J}}\times\mathbf{H}$ and $\mathbf{M}=-\mathbf{E}\times\hat{n}_{\mathrm{J}}$. The resulting systems can be written succinctly as

$$\mathsf{W}\begin{bmatrix}\mathbf{J}\sqrt{\eta_0}\\ -\mathbf{M}/\sqrt{\eta_0}\end{bmatrix}=\mathsf{W}q=-\mathsf{C}_1\mathsf{D}_1\Pi_{11}^{\mathrm{i}}q_{\mathrm{J}1}^{\mathrm{i}}+\sigma\mathsf{C}_2\mathsf{D}_1\Pi_{22}^{\mathrm{i}}q_{\mathrm{J}2}^{\mathrm{i}},\qquad \text{(A2)}$$

where $\eta_0=\sqrt{\mu_0/\varepsilon_0}$ is the intrinsic impedance of vacuum and the relevant operators are explicitly listed in Table A1. Moreover, in the light of (A1) and the definition of q in (A2), $q_{\mathrm{J}l}^{\mathrm{s}}$ are related to $q_{\mathrm{J}l}^{\mathrm{i}}$ and q via

$$q_{\mathrm{J}1}^{\mathrm{s}}=q_{\mathrm{J}1}^{\mathrm{i}}+\mathsf{D}_1q,\quad q_{\mathrm{J}2}^{\mathrm{s}}=q_{\mathrm{J}2}^{\mathrm{i}}-\mathsf{D}_2q.\qquad \text{(A3)}$$

Finally, deriving q from (A2) and substituting it into (A3), after a little algebra, yields the following operative expression for $\overline{\mathsf{S}}_{\mathrm{J}}$

$$\overline{\mathsf{S}}_{\mathrm{J}} = \begin{bmatrix} \mathsf{I}_{\mathrm{J}} - \mathsf{D}_1\mathsf{W}^{-1}\mathsf{C}_1\mathsf{D}_1\mathsf{\Pi}^{\mathrm{i}}_{11} & \sigma\mathsf{D}_1\mathsf{W}^{-1}\mathsf{C}_2\mathsf{D}_2\mathsf{\Pi}^{\mathrm{i}}_{22} \\ \mathsf{D}_2\mathsf{W}^{-1}\mathsf{C}_1\mathsf{D}_1\mathsf{\Pi}^{\mathrm{i}}_{11} & \mathsf{I}_{\mathrm{J}} - \sigma\mathsf{D}_2\mathsf{W}^{-1}\mathsf{C}_2\mathsf{D}_2\mathsf{\Pi}^{\mathrm{i}}_{22} \end{bmatrix}. \tag{A4}$$

The algebraic counterpart of $\overline{\mathsf{S}}_{\mathrm{J}}$ ensues by solving (A2) via MoM after expanding q with $2N_F$ RWG functions similarly to (7).

ACKNOWLEDGMENT

This research was supported by the post-doc fund under TU/e project No. 36/363450, and is performed in the framework of the MEMPHIS project (http://www.smartmix-memphis.nl/).

The authors would like to thank the Reviewers for their positive comments and useful remarks which helped improve the manuscript.

REFERENCES

1. Matekovitz, L., V. A. Laza, and G. Vecchi, "Analysis of large complex structures with the synthetic-functions approach," *IEEE Trans. Antennas Propag.*, Vol. 55, 2509–2521, Sep. 2007.
2. Ylä-Oijala, P. and M. Taskinen, "Electromagnetic scattering by large and complex structures with surface equivalence principle algorithm," *Waves in Random and Complex Media*, Vol. 19, 105–125, Feb. 2009.
3. Mittra, R. and K. Du, "Characteristic basis function method for iteration-free solution of large method of moments problems," *Progress In Electromagnetics Research B*, Vol. 6, 307–336, 2008.
4. Laviada, J., F. Las-Heras, M. R. Pino, and R. Mittra, "Solution of electrically large problems with multilevel characteristic basis functions," *IEEE Trans. Antennas Propag.*, Vol. 57, 3189–3198, Oct. 2009.
5. Xiao, G., J.-F. Mao, and B. Yuan, "A generalized surface integral equation formulation for analysis of complex electromagnetic systems," *IEEE Trans. Antennas Propag.*, Vol. 57, 701–710, Mar. 2009.
6. Harrington, R. F., *Field Computation by Moment Methods*, MacMillan, New York, 1968.
7. Bau III, D. and L. N. Trefethen, *Numerical Linear Algebra*, Soci. Indus. Ap. Math., Philadelphia, 1997.
8. Lancellotti, V., B. P. de Hon, and A. G. Tijhuis, "An eigencurrent approach to the analysis of electrically large 3-D structures using

linear embedding via Green's operators," *IEEE Trans. Antennas Propag.*, Vol. 57, 3575–3585, Nov. 2009.

9. Lancellotti, V., B. P. de Hon, and A. G. Tijhuis, "Electromagnetic modelling of large complex 3-D structures with LEGO and the eigencurrent expansion method," *AP/URSI Int. Symp.*, Charleston, SC, Jun. 2009.
10. Lancellotti, V., B. P. de Hon, and A. G. Tijhuis, "A total inverse scattering operator formulation for solving large structures with lego," *International Conf. on Electromagnetics in Advanced Applications, ICEAA'09*, 335–338, Sep. 2009.
11. Lancellotti, V., B. P. de Hon, and A. G. Tijhuis, "Sensitivity analysis of 3-D composite structures through linear embedding via Green's operators," *Progress In Electromagnetics Research*, PIER 100, 309–325, Jan. 2010.
12. Lancellotti, V., B. P. de Hon, and A. G. Tijhuis, "On the convergence of the eigencurrent expansion method applied to linear embedding via Green's operators," *IEEE Trans. Antennas and Propag.*, to appear.
13. Lancellotti, V., B. P. de Hon, and A. G. Tijhuis, "A priori error estimate and control in the eigencurrent expansion method applied to linear embedding via Green's operators," *AP/URSI Int. Symp.*, to be presented, Toronto, Canada, July 2010.
14. Lancellotti, V., B. P. de Hon, and A. G. Tijhuis, "Analysis of antennas in the presence of large composite 3-D structures with linear embedding via Green's operators (LEGO) and a modified EFIE," *4th EuCAP*, Barcelona, Spain, April 2010.
15. Kurz, S., O. Rain, and S. Rjasanow, "The adaptive cross-approximation technique for the 3D boundary-element method," *IEEE Trans. Magn.*, Vol. 38, 421–424, Mar. 2002.
16. Zhao, K., M. Vouvakis, and J.-F. Lee, "The adaptive cross approximation algorithm for accelerated method of moments computations of EMC problems," *IEEE Trans. Electromag. Compat.*, Vol. 47, 763–773, Nov. 2005.
17. Arnoldi, W. E., "The principle of minimized iterations in the solution of the matrix eigenvalue problem," *Quarterly of Applied Mathematics*, Vol. 9, 17–29, 1951.
18. Rao, S. M., D. R. Wilton, and A. W. Glisson, "Electromagnetic scattering by surfaces of arbitrary shape," *IEEE Trans. Antennas Propag.*, Vol. 30, 409–418, May 1982.
19. Collin, R. E., *Foundations for Microwave Engineering*, McGraw-Hill, New York, 1992.

20. Redheffer, R., "On the relation of transmission-line theory to scattering and transfer," *J. Math. Phys.*, Vol. 41, Mar. 1962.
21. Rumsey, V. H., "Reaction concept in electromagnetic theory," *Phys. Rev.*, Vol. 94, 1483–1491, Jun. 1954.
22. Harrington, R. F., *Time-harmonic Electromagnetic Fields*, McGraw-Hill, London, 1961.
23. Jackson, J. D., *Classical Electrodynamics*, 3rd edition, Wiley, Chichester, 1999.
24. Saad, Y., *Iterative Methods for Sparse Linear Systems*, 2nd edition, SIAM, 2003.
25. Golub, G. H. and C. F. van Loan, *Matrix Computations*, Johns Hopkins University Press, Baltimore, 1996.
26. Webb, D. B., E. Michielssen, and R. Mittra, "Thick frequency selective surfaces," *AP/URSI Int. Symp.*, Vol. 4, 1795–1798, Jul. 1992.
27. Love, A. E. H., "The integration of the equations of propagation of electric waves," *Philos. Trans. R. Soc. London, Ser. A*, Vol. 197, 1–45, 1901.
28. Poggio, A. J. and E. K. Miller, "Integral equation solutions of three dimensional scattering problems," *Computer Techniques for Electromagnetics*, Pergamon, Oxford, UK, 1973.
29. Ylä-Oijala, P. and M. Taskinen, "Well-conditioned Müller formulation for electromagnetic scattering by dielectric objects," *IEEE Trans. Antennas Propag.*, Vol. 53, 3316–3323, Oct. 2005.